Biosensors and Bioelectronics 33 (2012) 233–240

Contents lists available at SciVerse ScienceDirect

Biosensors and Bioelectronics

journal homepage: www.elsevier.com/locate/bios

Detection of uncharged or feebly charged small molecules by field-effect transistor biosensors

Chil Seong Ah[a,*], Chan Woo Park[a], Jong-Heon Yang[a], Joon Sung Lee[b], Wan-Joong Kim[a], Kwang Hyo Chung[a], Yo Han Choi[a], In Bok Baek[a], Jungho Kim[c], Gun Yong Sung[a]

[a] Biosensor Research Team, Electronics and Telecommunications Research Institute (ETRI), 218 Gajeong-ro, Yuseong-gu, Daejeon 305-700, Republic of Korea
[b] Medical Convergence Component Research Team, Electronics and Telecommunications Research Institute (ETRI), 218 Gajeong-ro, Yuseong-gu, Daejeon 305-700, Republic of Korea
[c] Graduate School of East-West Medical Science, Kyung Hee University, Yongin 446-701, Republic of Korea

ARTICLE INFO

Article history:
Received 3 November 2011
Received in revised form 4 January 2012
Accepted 9 January 2012
Available online 17 January 2012

Keywords:
Field-effect transistor
Nanoparticle charge
Mycotoxin
Signal enhancement
Small molecule detection

ABSTRACT

This paper describes a new technique for the detection of uncharged or feebly charged small molecules (<400 Da) using Si field-effect transistor (FET) biosensors that are signal-enhanced by gold nanoparticle (NP) charges under dry measurement conditions. NP charges are quickly induced by a chemical deposition (that is, Au deposition) and the indirect competitive immunogold assay, and strongly enhance the electrical signals of the FET biosensors. For the validation of signal enhancement of FET biosensors based on NP charges and detection of uncharged or feebly charged small molecules, mycotoxins (MTXs) of aflatoxin-B1 (AFB1), zearalenone (ZEN), and ochratoxin-A (OTA) were used as target molecules. According to our experimental results, the signal is 100 times more enhanced than the use of the existing solution FET biosensing techniques. Furthermore, this method enables the FET biosensor to quantitatively detect target molecules, regardless of the ionic strengths, isoelectric points (p*I*), or pHs of the measured sample solutions.

1. Introduction

Complementary metal oxide semiconductor (CMOS)-compatible field-effect transistor (FET) biosensors are useful tools for the diagnosis of various diseases, because they can electronically detect and analyze biomolecules, such as proteins, DNA, and small molecules, in real-time and with high sensitivity. Therefore, these biosensors have been the subject of many studies worldwide (Elfström et al., 2008; Ryu et al., 2010; Stern et al., 2007; Zheng et al., 2008; Zheng et al., 2005). In particular, CMOS-compatible FET biosensors that are produced by a top-down method utilize conventional semiconductor processes, which provide highly reproducible and uniform sensor characteristics that are suitable for mass production, however, despite the advantages of CMOS-compatible FET biosensors, most studies have been limited to the detection of biomolecules that have net electrical charges, such as proteins and DNAs (Elfström et al., 2008; Ryu et al., 2010; Stern et al., 2007; Zheng et al., 2008; Zheng et al., 2005). The FET approach for detecting small molecules, such as hormones, toxins, drugs, environmental pollutants, agrichemicals, and antibiotics is not applicable for a reproducible and portable sensor diagnosis because they are uncharged or feebly charged small molecules, despite their demands in many fields.

In addition to the difficulty of detecting small molecules that have no charge, other issues remain as obstacles to the utilization of FETs as suitable biosensors in diverse fields. First, it should be possible to measure signals under dry conditions so that the noise caused by the numerous redundant ions that are present in an aqueous solution can be eliminated. In previous studies (Ah et al., 2010; Elfström et al., 2008; Kim et al., 2010; Stern et al., 2007; Zheng et al., 2005), measurement in an aqueous environment was considered essential for keeping the net charges of the target biomolecules in a situation where the electrical signal of the FET element is easily affected by the ionic strength, p*I*, and pH of the sample solution. Second, the biomolecules need to be directly detectable in highly concentrated ionic solutions without dilution (Ah et al., 2010; Kim et al., 2010). With current FET sensor technology, it is difficult to analyze signals directly from highly ionic concentrated (~150 mM NaCl) physiological samples, such as human serum, because of the short Debye length (Stern et al., 2007) and varying pH and ion concentrations. Even if a sufficient Debye length is achieved by dissolving to desalt or dilute the sample (Stern et al., 2007; Zheng et al., 2005), it is still difficult to use pH solutions of controlled ion concentrations. Third, for 'top-down' fabrication techniques, enhancing sensitivity by reducing the channel dimension is limited because

* Corresponding author. Tel.: +82 42 860 1898; fax: +82 42 860 6594.
E-mail address: acs@etri.re.kr (C.S. Ah).

0956-5663/$ – see front matter © 2012 Elsevier B.V. All rights reserved.
doi:10.1016/j.bios.2012.01.010

complicated patterning processes, such as e-beam lithography, are required. Therefore, a new scheme for enhancing the signals to allow easy detection by a wide (sub-micron scale) channel is desirable to permit cost effective mass production of FET biosensors.

Mycotoxins (MTXs), such as aflatoxin-B1 (AFB1), zearalenone (ZEN), and ochratoxin-A (OTA), are typically uncharged or feebly charged small molecules (Fig. 1(a)) that are produced by fungal species, such as mushrooms, molds, and yeast, which are commonly found in cereals and nuts (Berthiller et al., 2005; el Khoury and Atoui, 2010; Wang and Wang, 2008). In contrast to other protein toxins, bacteria and viruses, MTXs have a lower molecular weight (300–400 Da), are poisonous at lower doses and are routinely found in food samples (AFB1: 2–8 ng/g-EU, ZEN: 20–200 ng/g-EU, and OTA: 2–10 ng/g-EU). MTXs have many negative health effects, in that they are carcinogenic, immunotoxic, nephrotoxic and teratogenic and are known to be endocrine disruptors. Toxins are conventionally analyzed using HPLC (Barfield et al., 2008; Berthiller et al., 2005), GC/MS (Alder et al., 2006; Barfield et al., 2008), ELISA (Nunes et al., 1998), and SPR (Mitchell et al., 2005). Despite their accuracy, these procedures require professional operators and expensive equipment and are time-consuming and complicated; therefore, they are not suitable for point-of-care testing (POCT) diagnosis that requires the rapid quantification of small molecule concentrations (Xiulan et al., 2005). Therefore, the development of quantitative, rapid, sensitive and specific assay techniques is needed for the routine analysis and monitoring of food, water, and air samples to test for natural and intentional contamination with these toxins.

2. Materials and methods

2.1. Fabrication of Si-FET devices

Si-FET sensors were fabricated using CMOS-compatible "top–down" processes from 8-inch silicon-on-insulator (SOI) wafers with an initial 100-nm-thick top silicon layer (8.5–22 Ω cm for the p- and n-type doped wafers). The initial top Si layer was thinned down to 40 nm by multiple dry oxidation and wet etching cycles and implanted with 1e13 cm^{-2} boron ions at 8 keV to form a p-type channel layer with a dopant concentration of 8e17 cm^{-3}, whereas it was implanted with 3e13 cm^{-2} phosphoric ions at 20 keV to form a n-type channel layer with a low or high doping concentration with a dopant concentration of 2e18 cm^{-3}. After the implanted boron or phosphorus atoms were activated at 950 °C for 30 min, the Si sensors that were 0.15–1 μm wide and 5–20 μm long were patterned by optical lithography using a KrF scanner and dry etching techniques. The regions of the Si contact leads were implanted with 2e15 cm^{-2} of boron or phosphoric ions, and they were rapidly annealed at 950 °C for 30 s to obtain good ohmic contact between the Si leads and the metal electrodes. The metal electrode was formed as a stack of Au/Cr/Al (50 nm/5 nm/50 nm) and was annealed at 400 °C for 30 min. Next, the metal electrodes were isolated from the aqueous solution by a 500-nm-thick SiN passivation layer that was deposited by plasma-enhanced chemical vapor deposition (PECVD) and patterned by lift-off. The surface RMS roughness of the Si-FET channel was measured by an atomic force microscope (Agilent 5500) and was less than 1 nm (Kim et al., 2007).

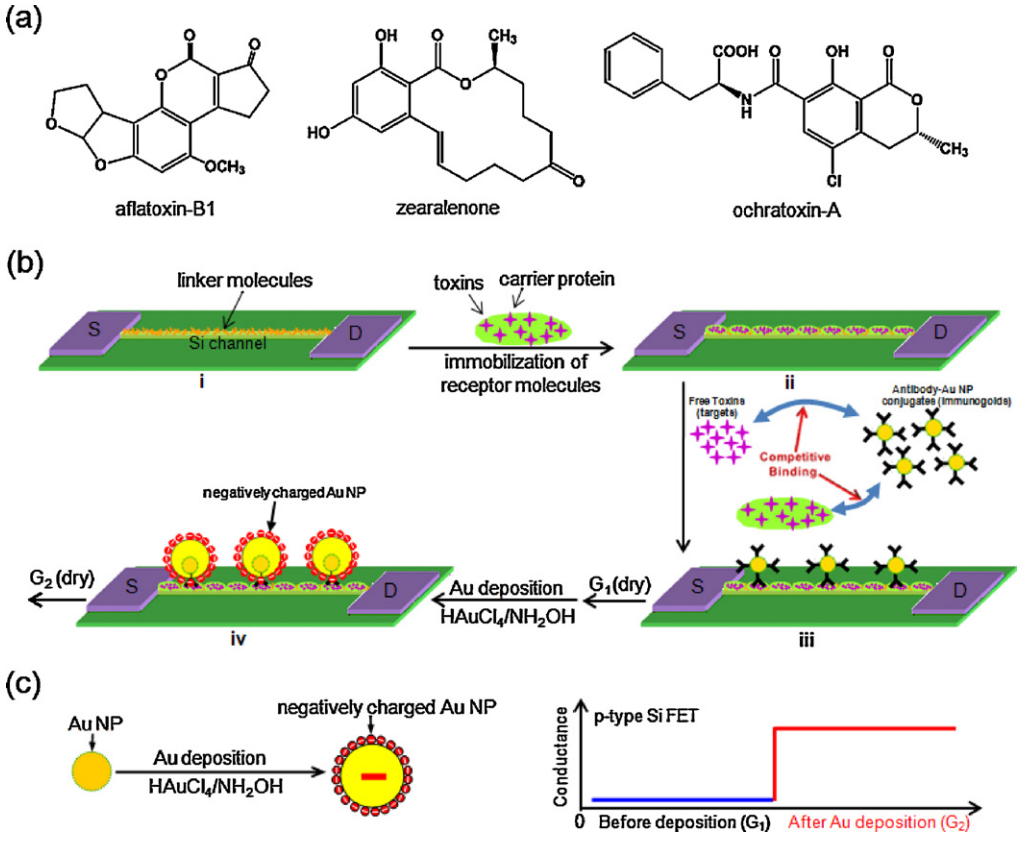

Fig. 1. Principles of detecting uncharged or feebly charged small MTX molecules. (a) Structures of the MTX molecules AFB1 (312 Da), ZEN (318.4 Da), and OTA (403.8 Da). (b) The indirect competitive immunogold assay for the immunogolds, receptor molecules that were immobilized onto the FET sensors, and MTX molecules. The generation of NP charges by NP growth is also shown. The NPs are grown using the Au deposition solution and strong charges occur on the sensor surface. (c) Gold NPs are grown using $HAuCl_4$ and NH_2OH solutions. Negative charges newly occur on the surface (left), resulting in a strong signal enhancement for p-type Si-FETs after Au deposition (right).

2.2. Immobilization of receptors of MTXs

Oxygen plasma treatment (42 Pa, 50 W, 5 min) was performed to produce a hydroxyl-terminated Si surface. The hydrophilic Si-FET surfaces were placed into a homemade Teflon reaction container with 200 μl of APTES (Sigma–Aldrich) under N_2. The container was heated to 120 °C for 10 min, and the functionalization of the Si-FET surface with APTES was verified. To bio-activate the surface for MTX-BSA (bovine serum albumin) or KLH (keyhole limpet hemocyanin) conjugate immobilization (Supporting Information Fig. S1), the APTES-functionalized chip was immersed in 25% glutaraldehyde (Sigma–Aldrich) that had been previously dissolved in DI water with 4 mM sodium cyanoborohydride ($NaBH_3CN$, Sigma–Aldrich) for 4 h, and the chip was then rinsed with DI water. The immobilization of the MTX-BSA (or KLH) conjugates was achieved by overnight exposure of the aldehyde-modified Si-FET to 100 μg/ml of the MTX-BSA (or KLH) conjugates in a 10 mM phosphate buffer solution (pH 8.4) containing 4 mM $NaBH_3CN$. To block the unreacted aldehyde, the device was immersed in a 1% casein solution (10 mM phosphate buffer, pH 8.4; 10% casein blocker; Pierce) with 4 mM $NaBH_3CN$ for 30 min. The conjugates-immobilized chip was sequentially washed with 0.05% Tween in 1× PBS two times, and 1× PBS three times.

2.3. MTX samples

AFB1 and AFB1-BSA conjugates were purchased from Sigma (ca#: A6636 and A6655, respectively). ZEN was purchased from Sigma (ca#: Z2125), and ZEN-KLH conjugates were received from Standard Diagonostics (SD Company, Korea). OTA and OTA-BSA conjugates were purchased from Sigma (ca#: O1877 and O3007, respectively). Mab-AFB1, ZEN, and OTA were received from SD Company.

2.4. Indirect competitive immunogold assay

The immunogolds were prepared as described previously (Hermanson, 1996; Kim et al., 2010) by the conjugation of gold nanoparticles (NPs) (BBI International, 10 nm in diameter) with mabs of MTXs (mouse-mab-AFB1, mouse-mab-ZEN, and mouse-mab-OTA provided by Standard Diagnostics). The synthesized immunogolds were diluted to 4.5 nM in a 1× PBS buffer. The purchased MTXs (AFB1, ZEN, and OTA) were dissolved in 70% methanol and diluted with 1× PBS (10 mM phosphate, 138 mM NaCl, 2.7 mM KCl, and pH 7.4; Sigma–Aldrich) to various concentrations, depending on the purpose of the experiment. The MTX-carrier protein-immobilized FET sensor surface was incubated within the MTX and immunogold solutions at room temperature for 45 min by spotting. The Au NPs captured Si chips were sequentially rinsed with 0.0001× PBS and water and dried with N_2 gas.

2.5. Au deposition and electrical measurements

The Au NPs captured Si-FET chip was loaded onto the electrical measurement system along with a manipulator, a fluidic channel, and probe cards for reading different Si-FET sensors simultaneously. The developed sensor was electronically measured in real time using the previously described AC lock-in amplifier (f = 79.83 Hz, V_{p-p} = 50 mV) (Stanford Research Systems, SR830) (Kim et al., 2010). Injection of Au deposition solutions prepared by mixing 10 mM $HauCl_4{\cdot}3H_2O$ and 16 mM $NH_2OH{\cdot}HCl$ (1:1) were performed through a PDMS (polydimethylsiloxane) microfluidic channel (500 μm width and 240 μm height) that was loaded onto the Au NPs captured Si-FET chip at a flow rate of 900 μl/min using a syringe pump (KDS-200, KD Scientific). All electrical measurements (G_1 and G_2) were performed in air environment, i.e. dried atmosphere (Ryu et al., 2010; Seo et al., 2006) before and after the Au deposition reactions. G_1 and G_2 are conductance values before and after the Au deposition reactions, respectively. The before and after levels were obtained by averaging conductance values after current stabilization.

2.6. Kelvin probe force microscopy (KPFM) and X-ray photoelectron spectroscopy (XPS)

The KPFM measurements were with a KP-6500 (McAllister Technical Services) Kelvin probe system placed on a vibrationally isolated table. The XPS experiments were performed with a ESCALAB 200R (Thermo electron (VG Scientific)) photoelectron spectrometer with a monochromatized Al Kα X-ray source (1486.6 eV) operated at 12.5 kV, 20 mA, and 250 W at a base pressure of 5×10^{-10} Torr. Photoelectrons were collected at an angle of 70° relative to the surface normal.

3. Results and discussion

The detection of uncharged or feebly charged small MTX molecules by Si-FET sensors involves NP growth and indirect competitive immunogold assay of the subsequent NP conjugates (monoclonal antibody (mab)-MTXs-Au NPs conjugates, immunogolds), that is to say, the receptor molecules (MTXs-carrier protein conjugates) (Supporting Information Fig. S1) that are immobilized onto the FET sensor, and the target MTX molecules are detected (Fig. 1(b)). 3-aminopropyltriethoxysilanes (APTESs) were used as a linker to immobilize the receptor molecules onto the Si-FET sensor (step i → step ii) (Kim et al., 2007). The immunogolds specifically and competitively bind with the sample target MTXs or receptor molecules that are immobilized on the active area of the Si-FET sensor (step ii → step iii). If there are more MTXs in the sample, fewer NPs are captured on the surface of the FET sensor, whereas more NPs are captured when there are fewer MTXs (step iii) (Supporting Information Fig. S2). Next, the captured NPs immediately are grown and charged through an Au deposition reaction (step iii → step iv). As a result, the grown NPs have acquired new, strongly negative charges and cause abrupt signal enhancement for the conductance between the source and the drain electrodes of the p-type Si-FET (Fig. 1(c)). In the case of p-type Si-FET, a negative gate voltage induces the accumulation of majority charge carriers (holes), increasing the channel conductance. However, a positive gate voltage leads to the depletion of holes and reduces the conductance. The new creation of the negatively charged Au nanoparticles is equivalent to the application of a negative gate voltage, and results in an increase of conductance of the p-doped Si nanochannel.

The Si-FET biosensors were fabricated on a CMOS-compatible 8-inch wafer. A single chip has 4 identical groups of sensors, and each group has 8 sensors with different dimensions. The current–voltage curves between the source and the drain of the 32 sensors on one chip exhibit small deviations with a good linearity (Supporting Information Fig. S3). To find the degree of signal enhancement induced by the NP charges, we conducted AFB1 detection experiments depending on the Au deposition reaction time under dry conditions, immediately after immunogold assay (Fig. 2). The detection signal of 1 ng/ml of AFB1 was obtained after immunogold assays followed by 0, 30, and 90 s of Au deposition. The concentration of immunogold was 4.5 nM. After the immunogold assay, 500 NPs per 1 μm^2 was present on the Si-FET sensor, and the size of the NPs increased as the Au deposition time increased (upper three SEM images, Fig. 2(a)). No NPs were observed on the IgG-immobilized sensors, suggesting that there was little non-specific binding. Also, no NPs were found after the Au deposition reaction was carried out without NPs (lower three SEM images, Fig. 2(a)). AFB1-BSA and IgG were separately immobilized onto

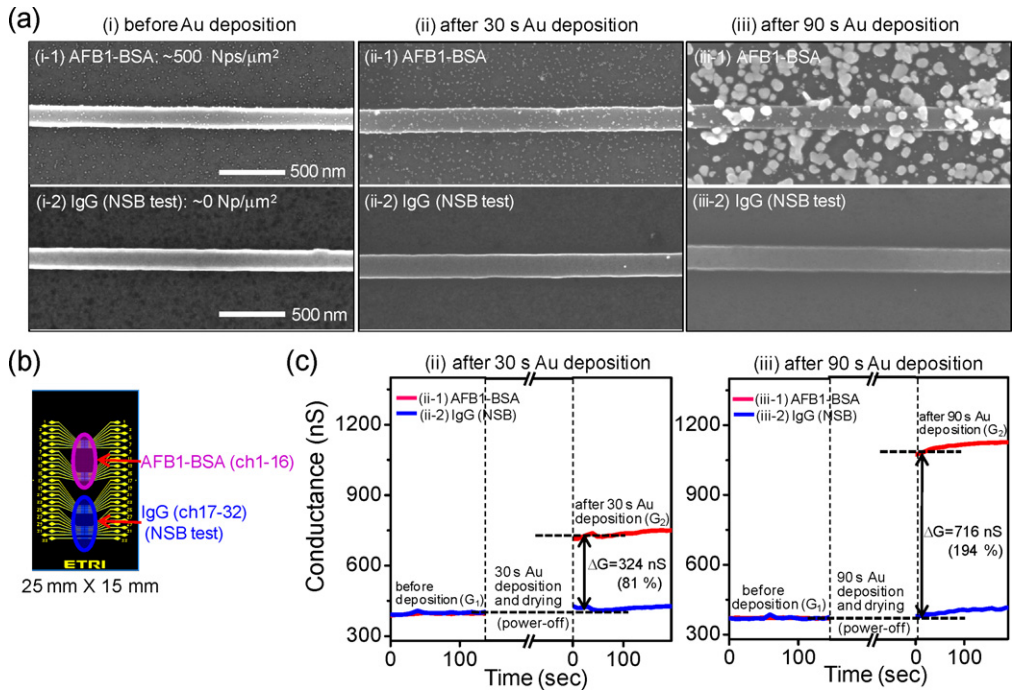

Fig. 2. Signal enhancements by the NP charges. (a) SEM images taken before Au deposition (chip i), after 30 s (chip ii) of Au deposition, and after 90 s (chip iii) of Au deposition. AFB1-BSA and IgG were separately immobilized on one chip. AFB1-BSA specifically combines with immunogolds at an AFB1 concentration of 1 ng/ml, and IgG is used to test for nonspecific binding. Five hundred NPs specifically combined on 1 μm^2 of the AFB1-BSA sensor (upper three SEM images, 0, 30, and 90 s), and very few NPs were identified on the IgG sensor (lower three SEM images, 0, 30, and 90 s). (b) Layout of the reaction chip, which consisted of 32 Si-FET sensors. AFB1-BSA was immobilized by spotting on Si-FET sensors 1–16, and IgG was immobilized on sensors 17–32. (c) Conductance vs. time data corresponding to (a). The p-type Si-FET was doped with 1e13 cm^{-2} boron ions at 8 keV. The dimensions of the measured Si-FETs were 180 nm × 5 μm × 40 nm (W/L/H).

one FET chip (Fig. 2(b)). AFB1-BSAs that specifically combined with immunogolds were immobilized by spotting onto one half (sensors 1–16) of the Si-FET chip and, to perform a nonspecific binding test, IgG molecules that do not react with immunogolds were immobilized onto the other half (sensors 17–32). The Au deposition reaction was performed by flowing a solution, which was prepared by mixing 10 mM $HAuCl_4 \cdot 3H_2O$ and 16 mM $NH_2OH \cdot HCl$ at 1:1 ratio at the rate of 900 (l/min through the PDMS channel (width/height: 500 μm/240 μm). Almost no NPs and no absorbance appeared when the two solutions were mixed in the absence of NPs, and NP growth was limited to those cases where NPs were already present (Fig. 2(a) and Supporting Information Fig. S4). A conductance change (ΔG) of 324 nS (81% signal increase) was observed after 30 s of Au deposition, and a ΔG of 716 nS (194% signal increase) was observed after 90 s (Fig. 2(c)). The signal enhancement became larger when the NP size became larger because of longer Au deposition. The measured signal (ΔG) was obtained from the difference between the conductance (G_1) before Au deposition and the conductance (G_2) after Au deposition.

Fig. 3 shows the plots of conductance vs. time for AFB1 detection that were measured in an aqueous environment when performing the immunogold assay (Fig. 3(a)) using methods that have previously been described (Ah et al., 2010; Kim et al., 2010). This experiment was conducted to check how the signals are enhanced by NP charges under dry conditions in comparison with signals in aqueous environments. The reference buffer (10 μM phosphate buffer, pH of 5.8) was flowed in regions 1 and 3. The buffer flow in region 1 was used to set the initial conductance (G_1), whereas the flow in region 3 was established to remove any remaining reaction solution from region 2 and to set the final conductance (G_2). As previous studies (Kim et al., 2010), the measured signal (ΔG) was derived from the difference between G_1 and G_2. The reaction solution contained 4.5 nM immunogolds and 1 ng/ml of AFB1 (in 1× PBS). In the region 2, an immunogold assay was performed. AFB1-BSA and IgG were separately immobilized onto a single chip to test specific and nonspecific binding. At a pH of 5.8, mab-AFB1 (p*I* ~8–9) (Hermanson, 1996) is positively charged. Thus, if the mab-AFB1 of immunogolds is bound to the ABF1-BSA, the depletion of holes occurs within the p-type Si channel, and the conductance is decreased. ΔG was 10 nS and $\Delta G/G_1$ was 2.3% for the AFBA-BSA immobilized FET sensors, whereas ΔG was 0 nS and $\Delta G/G_1$ was 0% for the IgG immobilized FET sensors for non-specific binding test. Fig. 3(b) depicts an SEM image that was taken from the same sensors that were measured in Fig. 3(a), wherein SEM analysis was performed immediately after real-time analysis in the solution. NPs (500 per 1 μm^2) were observed on the AFB1-BSA sensor, and no NPs were observed on the IgG sensor. In other words, despite the sufficient specific binding of NP conjugates, a low signal was observed in this solution system in comparison with the dry system. Notably, NP charges under dry conditions (ΔG = 716 nS (194%) in Fig. 2(c)) increased the signals by about 100 times of magnitude over that of the signal measured in the aqueous solution (ΔG = 10 nS (2.3%) in Fig. 3(a)).

NP charges enable the distinct quantitative concentration analysis of AFB1 under dry conditions (Fig. 4(a)–(c)). Detection tests were performed for AFB1 concentrations of 0.5, 10, 20, and 100 ng/ml for p-type Si-FET chips. After Au deposition, the conductance clearly and quantitatively decreased as the AFB1 concentration increased (filled columns, Fig. 4(a)). Although we can see that the number of NPs on the Si-FET biosensors for SEM images before Au deposition quantitatively decreased as the AFB1 concentration increased (Supporting Information Fig. S2), the initial conductances before Au deposition do not show the concentration dependency of the AFB1, and also are not even in the conductance values of 900–1150 nS (open columns, Fig. 4(a)). The conductances after Au deposition for all of the AFB1 concentrations quantitatively decreased, and also the conductance changes (ΔG) (Fig. 4(b)) and the ratio of the conductance change ($\Delta G/G_1$) (Fig. 4(c)) quantitatively decreased as a

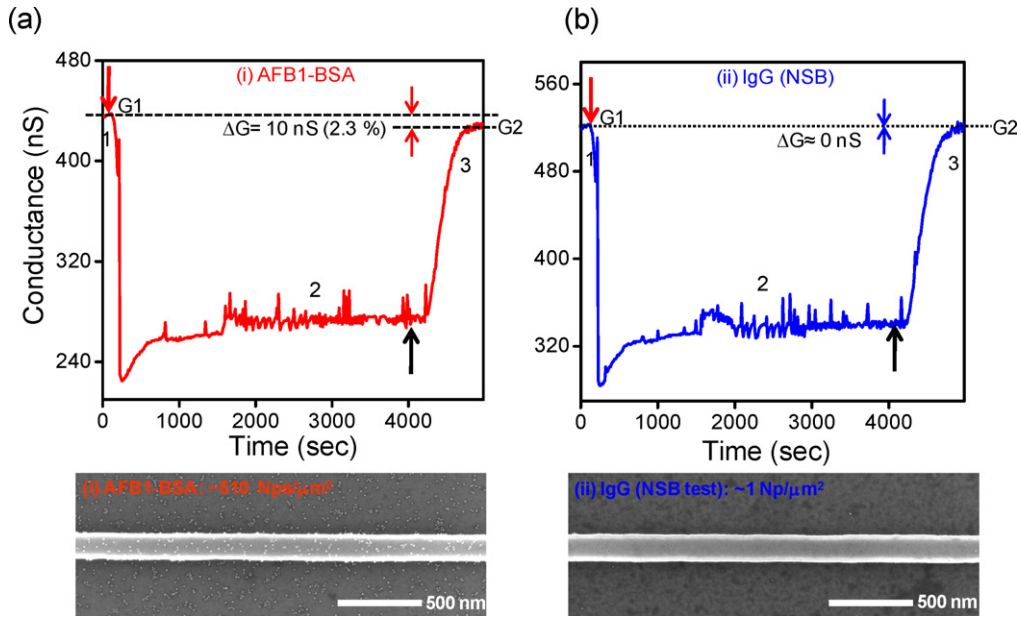

Fig. 3. The plots of conductance vs. time for AFB1 detection in 1× PBS reaction solution by (a) an AFB1-BSA- and (b) IgG-immobilized p-type Si-FET biosensor. The reference buffer was a 10 μM phosphate buffer (pH 5.8) and was flowed in regions 1 and 3. The buffer flow in region 1 was used to set the initial conductance G_1, and the flow in region 3 was established to remove the remaining solution from region 2 and to set the conductance G_2. For the immunogold assay in region 2, a reaction buffer solution (1× PBS) containing 1 ng/ml AFB1 and immunogolds was added. The measured signal (ΔG) was calculated from the difference between G_1 and G_2. SEM images of the sensors was measured for respective biosensors. The dimensions of the measured Si-FETs were 180 nm × 5 μm × 40 nm (W/L/H).

function of increasing AFB1 concentration. Even though the initial conductance levels of the p-type Si-FET chips were not even (a coefficient of variation of ~11% for 16 sensors of the same dimension), it was possible to quantitatively analyze AFB1 concentrations because of the substantial increase of the conductance after Au deposition.

For the complementary sensing of AFB1 by n-type Si-FETs, the n-type channel conductance was measured at AFB1-concentration

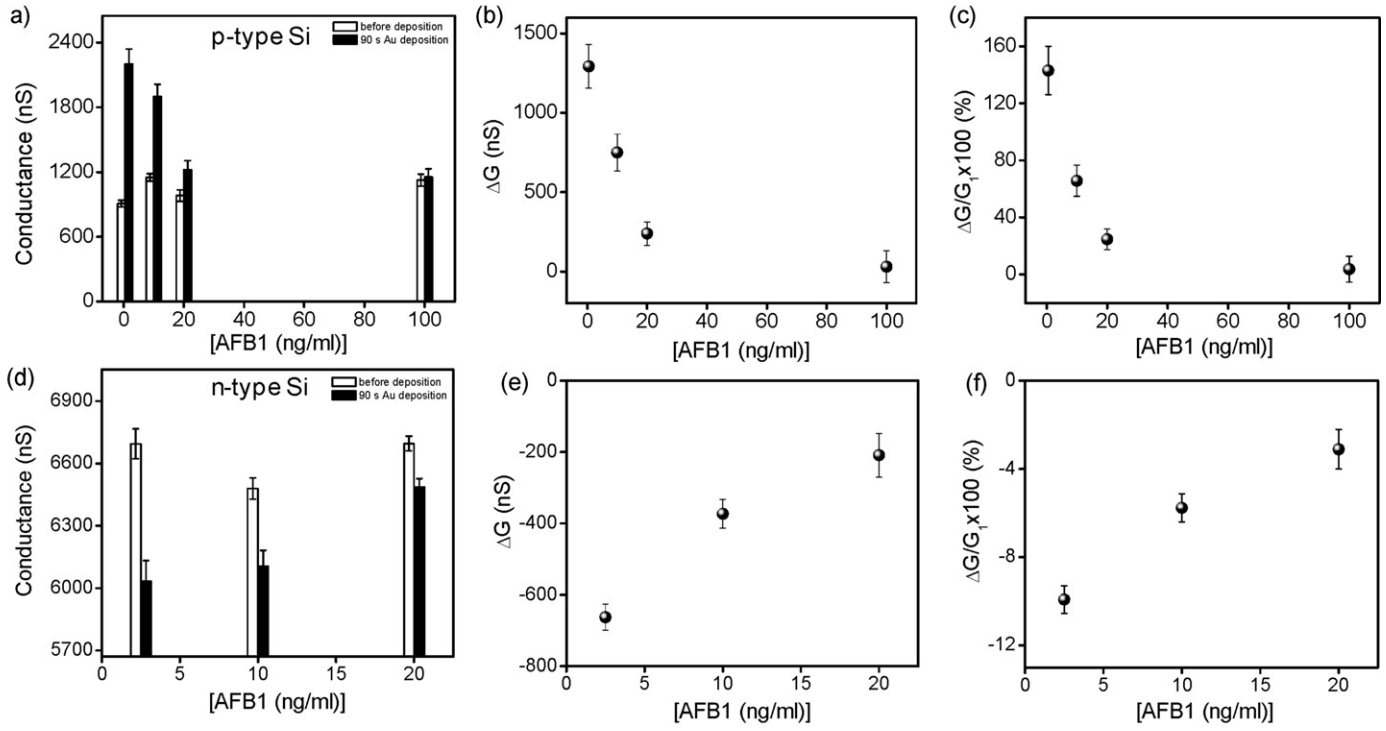

Fig. 4. The quantitative concentration detection of AFB1 for p-type Si-FET sensors. (a) AFB1 concentration-dependent conductance before (open columns) and after (filled columns) Au deposition and (b) the conductance changes (ΔG), and (c) the ratio of the conductance change ($\Delta G/G_1$) for p-type Si-FETs. All conductance values increased in a positive direction. The measured AFB1 concentration levels were 0.5, 10, 20, and 100 ng/ml. The p-type Si-FET was doped with 1e13 cm^{-2} boron ions at 8 keV. (d) The AFB1 concentration-dependent conductance before (open columns) and after (filled columns) Au deposition (left panel), (e) the ΔG and (f) the $\Delta G/G_1$ for the n-type Si-FET sensors. All conductance values decreased in a negative direction. The measured AFB1 concentrations were 2.5, 10, and 20 ng/ml. The n-type Si-FET was doped with 3e13 cm^{-2} phosphoric ions at 20 keV. The dimensions of the measured Si-FETs used were 300 nm × 5 μm × 40 nm (W/L/H).

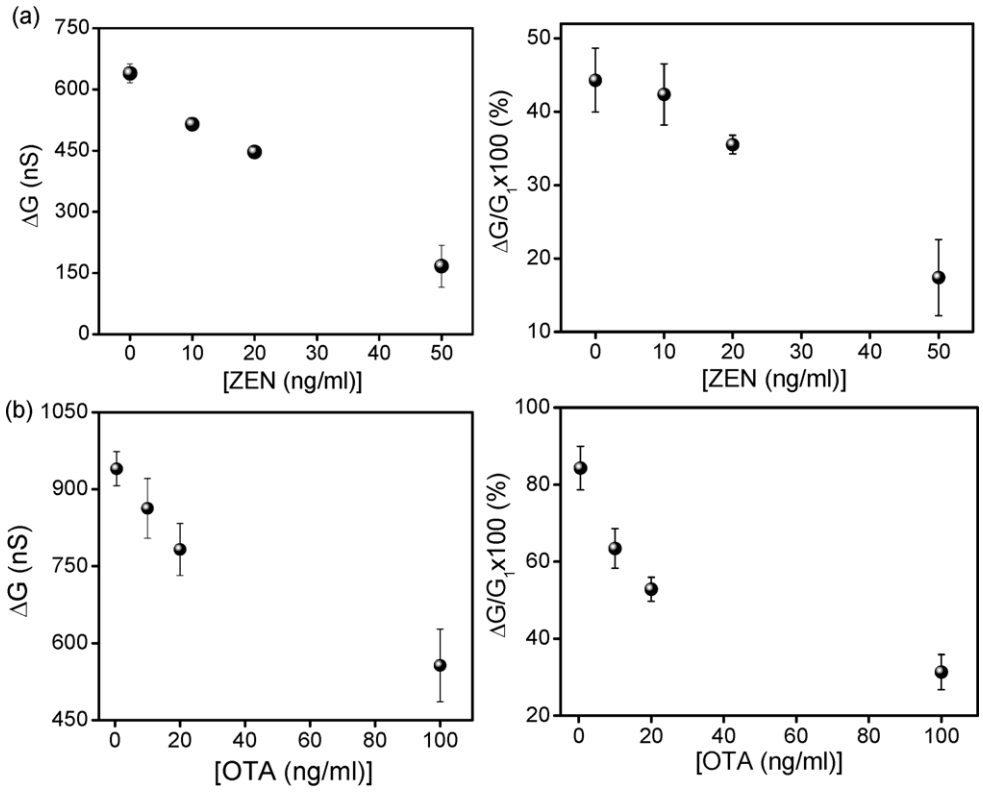

Fig. 5. The quantitative concentration detection of ZEN and OTA. (a) The ΔG (left) and the $\Delta G/G_1$ (right) for various ZEN concentrations. The measured ZEN concentrations were 0.5, 10, 20, and 50 ng/ml. (b) The ΔG (left) and the $\Delta G/G_1$ (right) according to OTA concentrations. The measured OTA concentrations were 0.5, 10, 20, and 100 ng/ml. The p-type Si-FET was doped with 1e13 cm^{-2} boron ions at 8 keV. The dimensions of the measured Si-FETs were 300 nm × 5 μm × 40 nm (W/L/H).

levels of 2.5, 10, and 20 ng/ml (Fig. 4(d)–(f)). The conductance values for all of the AFB1 concentration levels decreased after Au deposition (filled columns, Fig. 4(d)), and the ΔG and the $\Delta G/G_1$ decreased as a function of increasing AFB1 concentration (Fig. 4(e) and (f)). But, also the initial conductance measured before deposition was in the range of 6480–6700 nS with no dependence on the AFB1 concentrations (open columns, Fig. 4(d)). The initial conductance of the n-type Si-FET was higher than that of the p-type Si-FET owing to its increased (3 times higher) doping level (see Section 2). The conductance increased for the p-type Si-FET and decreased for the n-type Si-FET, which demonstrated that the grown NPs had negative charges under dry measurement conditions. In addition, as the sensor dimension decreases, the $\Delta G/G_1$ increases and the ratio of the conductance change reaches about 2000% at max. (Supporting Information Fig. S5). Fig. 5 shows the conductance change vs. concentration for two other food MTXs, ZEN and OTA. Fig. 5(a) shows the concentration analysis data for ZEN toxins. Samples with ZEN concentrations of 0.5, 10, 20, and 50 ng/ml were measured for p-type Si-FET chips. The ΔG was observed to decrease as the ZEN concentration increased, and also the $\Delta G/G_1$ decreased with increasing ZEN concentrations. Fig. 5(b) depicts the results from a similar analysis of OTA at concentrations of 0.5, 10, 20, and 100 ng/ml. The trends of the results from the OTA toxin experiment were similar to those obtained from the ZEN toxin experiment.

In the complementary sensing experimental of AFB1 using p- and n-type Si-FETs, we demonstrated that the grown NPs are negatively charged. There were some previous examples that NPs are positively or negatively charged by chemical or physical methods in solutions or air conditions (Cho et al., 2009; Suh et al., 2005; Zhang et al., 2007). However, to make sure the charge status of the NPs, we performed additional experiments. In the first experiment, the charge status of the grown NPs in the solution was identified. The movements of grown NPs within the solution were checked while applying a DC voltage between two FTO (fluorine-doped tin oxide, SnO_2:F on glass) electrodes (Fig. 6(a) and Supporting Information Fig. S6). As a result, after Au deposition, the grown NPs clearly moved toward the positive (+) electrode, whereas grown NPs were not observed around the negative (−) electrode (Supporting Information Fig. S7). The movement of the NPs toward the positive electrode revealed that the grown NPs were negatively charged. In the second experiment, the charge status of the grown NPs under dry conditions was identified: the contact potential difference (CPD) and work function of the stained Au was measured using KPFM (Fig. 6(b)) (Palermo et al., 2006; Tsai et al., 2011; Yu et al., 2009). Gold films evaporated onto bulk Si substrates was used. The CPD value of the gold film was decreased by 90 mV after Au deposition. This decrease in the CPD and the corresponding increase of the work function suggest that negative charges have been created on the gold surface as a result of Au deposition. The third experiment examined the charge status of the grown NPs by measuring the surface zeta potential (Supporting Information Fig. S8). After conducting an immunogold assay of a 0.5 ng/ml AFB1 concentration, the initial potential before Au deposition (−11 mV) changed to −32 mV after Au deposition, which is a decrease of approximately 21 mV. The negative change demonstrated that negative charges were created.

The XPS before and after Au deposition was also measured to verify the composition of the newly created negative charges on the grown NPs. Gold films evaporated onto bulk Si substrates were used. A new chloride peak appeared at 198 eV after 90 s of Au deposition (Fig. 6(c)), and this peak was not visible before Au deposition (Supporting Information Fig. S9). The newly created negative charges are suspected to have been caused by chloride. The reduction reaction of $HAuCl_4$ that was caused by the addition of NH_2OH to the gold surface occurs as follows (Ah et al., 2006), in the reaction mixture, protonated hydroxylamine initially adsorbs on

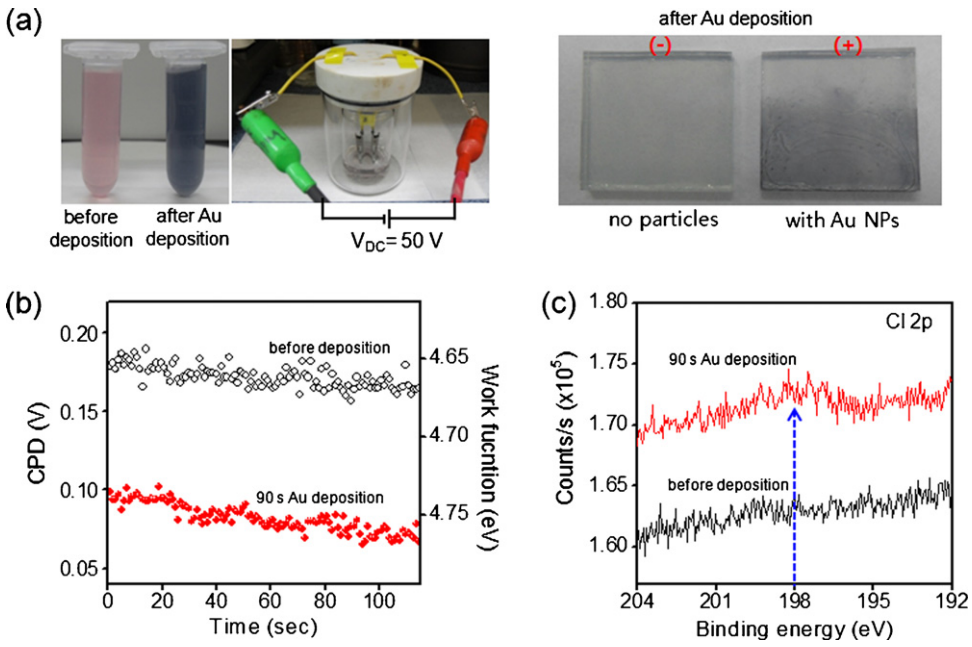

Fig. 6. Verification of the charge status of NPs. (a) Pictures of the Au NP solution before (red) and after (blue) Au deposition and the application of a DC voltage (50 V, 5 min) after two FTO electrodes were dipped in the NP solution (left). The distance between the electrodes was 1 cm, the width of the electrodes was 1 cm^2, and the current was 0.6–0.8 mA. The images on the right show the negative (−) and positive (+) electrodes after the application of the DC voltage of the grown Au NP solution. (b) The contact potential difference (CPD) and work function was measured by KPFM before (black) and after (red) Au deposition to identify the charge status of the NPs under dry conditions. Gold films evaporated onto bulk Si substrates was used. The work function of the calibrated probe tip was 4.834 eV. (c) The XPS data before (black) and after (red) Au deposition of gold films evaporated onto bulk Si substrates. A chloride peak at a binding energy of 198 eV appeared after Au deposition. (For interpretation of the references to color in this figure legend, the reader is referred to the web version of the article.)

the metal surfaces and oxidizes into adsorbed NO($H_3NOH^+ \rightleftarrows H_3NOH^+_{ads}$, $H_3NOH^+_{ads} \rightleftarrows H_2NO_{ads} + 2H^+ + e^-$, $H_2NO_{ads} \rightarrow HNO_{ads} + H^+ + e^-$, and $HNO_{ads} \rightleftarrows NO_{ads} + H^+ + e^-$). The reduction of Au^{3+} ions to Au^0 occurs as follows: $AuCl_4^- + 2e^- \rightleftarrows AuCl_2^- + 2Cl^-$, $3AuCl_2^- \rightleftarrows AuCl_4^- + 2Au^0 + 2Cl^-$, and $AuCl_2^- + e^- \rightleftarrows 2Au^0 + 2Cl^-$. Consequently, the generation of ions such as $AuCl_4^-$, $AuCl_2^-$, or Cl^- on the surface should be possible (Pérez-Juste et al., 2005).

The biomolecule sensing technology using CMOS-compatible Si-FET biosensors that utilize NP charges discussed herein enabled the electrically and reproducibly quantitative detection of uncharged or feebly charged small molecules at certain concentration ranges. In this study, NP charges were quickly induced by a chemical deposition (that is, Au deposition) and the indirect competitive immunogold assay. It was possible to analyze small MTXs molecule using large-sized FET biosensors (sub-micron scale) in dry conditions regardless of the p*I*, pH, and ionic strengths of the samples. The Si-FET biosensors were made using CMOS-compatible semiconductor processes, and many sensors of the same dimensions were fabricated on a chip to improve the reproducibility of the sensor signals. The size of the NPs and the quantity of the electric charges increased as the Au deposition time was prolonged. To verify the complementary signal changes between p-type and n-type Si-FET biosensors, concentration-dependent experiments were performed for various AFB1 concentrations. All of the investigated p-type Si-FET biosensors showed an increase in conductance with decreasing AFB1 concentration and prolonged deposition times, whereas the results with the n-type Si-FET biosensors exhibited the opposite trend. The measurement of NP charges using the dry conditions method resulted in a signal enhancement that was higher, by two orders of magnitude, than that of the electric signals that were measured in solutions system. In addition, stable quantitative concentration analysis of the target MTX molecules of AFB1, ZEN, and OTA was possible because of the enhanced signals that resulted from the charging of the NPs by Au deposition.

Additional experiments were performed to observe the charge status of grown NPs. When a DC voltage was applied between the FTO electrodes, the grown NPs were found to move toward the positive electrode, suggesting the negative charging of the NPs. The KPFM results, along with the surface zeta potential and XPS measurement results, also suggested that outward surface dipoles consisting of negatively charged chloride ions covered the Au NPs surfaces. The induced charge redistribution in the NPs that was caused by the surface dipoles may be responsible for the high conductance changes in the Si-FET channels below.

4. Conclusions

We have proposed a new technique for the detection of uncharged or feebly charged small molecules (<400 Da) using Si-FET biosensors that are signal-enhanced by gold NP charges. This measurement was carried out under dry conditions, and NP charges enabled the FET biosensor to quantitatively detect, regardless of the ionic strength, p*I*, or pH of the samples, uncharged or feebly charged small MTXs of AFB1, ZEN, and OTA with reproducibility, which have been difficult to detect with existing solution FET biosensing techniques. The biosensing signals induced by the NP charges under dry conditions were enhanced by two orders of magnitude in comparison with the signals that were measured in solution. A new scheme for enhancing signals that are detectable by wide (sub-micron scale) channel FETs is desirable because it would permit the mass production of this technology and also, Si-FET biosensor using NP charges proposed in this work should have the potential to become one of the popular POCT technologies for detecting of small molecules in the near future.

Acknowledgments

This work was partly supported by the Ministry of Knowledge Economy in Korea [2009-F-008-01, Programmable Bio-CMOS Field-Effect Transistors] and the Smart IT Convergence System Research Center funded by the Ministry of Education, Science and Technology as Global Frontier Project (SIRC-2011-0031866). The authors would like to thank Miss Cho Hee Lee for her technical supports.

Appendix A. Supplementary data

Supplementary data associated with this article can be found, in the online version, at doi:10.1016/j.bios.2012.01.010.

References

Ah, C.S., Yun, Y.J., Lee, J.S., Park, H.J., Ha, D.H., Yun, W.S., 2006. Appl. Phys. Lett. 88, 133116.
Ah, C.S., Kim, A., Kim, W.-J., Park, C.W., Ahn, C.-G., Yang, J.-H., Baek, I.B., Kim, T.-Y., Sung, G.Y., 2010. Bull. Korean Chem. Soc. 31 (6), 1561–1567.
Alder, L., Greulich, K., Kempe, G., Vieth, B., 2006. Rev. Mass Spetrom. 25, 838–865.
Barfield, M., Spooner, N., Lad, R., Parry, S., Fowles, S., 2008. J. Chromatogr. B 870, 32–37.
Berthiller, F., Schuhmacher, R., Buttinger, G., Krska, R., 2005. J. Chromatogr. A 1062, 209–216.
Cho, E.C., Xie, J., Wurm, P.A., Xia, Y., 2009. Nano Lett. 9 (3), 1080–1084.
el Khoury, A., Atoui, A., 2010. Toxins 2, 461–493.
Elfström, N., Karlström, A.E., Linnros, J., 2008. Nano Lett. 8 (3), 945–949.
Hermanson, G.T., 1996. Bioconjugate Techniques. Academic Press, California.
Kim, A., Ah, C.S., Yu, H.Y., Yang, J.-H., Baek, I.-B., Ahn, C.-G., Park, C.W., Jun, M.S., 2007. Appl. Phys. Lett. 91, 103901.
Kim, A., Ah, C.S., Park, C.W., Yang, J.-H., Kim, T., Ahn, C.G., Park, S.H., Sung, G.Y., 2010. Biosens. Bioelectron. 25, 1767–1773.
Mitchell, J.S., Wu, Y., Cook, C.J., Main, L., 2005. Anal. Biochem. 343, 125–135.
Nunes, G.S., Toscano, I.A., Barceló, D., 1998. Trends Anal. Chem. 17 (2), 79–87.
Palermo, V., Palma, M., Samorì, P., 2006. Adv. Mater. 18, 145–164.
Pérez-Juste, J., Pastoriza-Santos, I., Liz-Marzán, L.M., Mulvaney, P., 2005. Coord. Chem. Rev. 249, 1870–1901.
Ryu, S.-W., Kim, C.-H., Han, J.-W., Kim, C.-J., Jung, C., Park, H.G., Choi, Y.-K., 2010. Biosen. Bioelectron. 25, 2182–2185.
Seo, K.-I., Sharma, S., Yasseri, A.A., Stewart, D.R., Kamins, T.I., 2006. Electrochem. Solid-State Lett. 9 (3), G69–G72.
Stern, E., Klemic, J.F., Routenberg, D.A., Wyrembak, P.N., Turner-Evans, D.B., Hamilton, A.D., LaVan, D.A., Fahmy, T.M., Reed, M.A., 2007. Nature 445, 519–522.
Suh, J., Han, B., Okuyama, K., Choi, M., 2005. J. Colloid Interface Sci. 287, 135–140.
Tsai, C.-C., Chiang, P.-L., Sun, C.-J., Lin, T.-W., Tsai, M.-H., Chang, Y.-C., Chen, Y.-T., 2011. Nanotechnology 22, 135503 (9pp).
Wang, X.-H., Wang, S., 2008. Sensors 8, 6045–6054.
Xiulan, S., Xiaolian, Z., Jian, T., Zhou, J., Chu, F.S., 2005. Intern. J. Food Microbiol. 99, 185–194.
Yu, Y.-J., Zhao, Y., Ryu, S., Brus, L.E., Kim, K.S., Kim, P., 2009. Nano Lett. 9 (10), 3430–3434.
Zhang, L., Yuan, R., Chai, Y., Li, X., 2007. Anal. Chim. Acta 596, 99–105.
Zheng, G., Patolsky, F., Cui, Y., Wang, W.U., Lieber, C.M., 2005. Nat. Biotechnol. 23 (10), 1294–1301.
Zheng, G.-J., Zhang, G., Chua, J.H., Chee, R.-E., Wong, E.H., Agarwal, A., Buddharaju, K.D., Singh, N., Gao, Z., Balasubramanian, N., 2008. Nano Lett. 8 (4), 1066–1070.